CrossMark

Effects of sintering atmospheres on thermoelectric properties, phase, microstructure and lattice parameters c/a ratio of Al, Ga dual doped ZnO ceramics sintered at high temperature

Matiullah[1] · C.L. Wang[1,2] · W. B. Su[1] · A. Zaman[3] · Ikram Ullah[4] · J. Z. Zhai[1] · D. K. Liu[1]

Abstract

Thermoelectric properties, phase and microstructural investigation of $(Zn_{1-x-y}Al_xGa_y)O$, where x = 0.02, y = 0.04, 0.05 and x = 0.03, y = 0.01, 0.02 are studied at a high temperature of 1450 °C in this article. We have focused on the effects of sintering atmospheres on thermoelectric properties, phase, and microstructure in the air as well in the argon atmosphere. The Seebeck coefficient (S) and electrical resistivities (ρ) measured in air and argon atmospheres have an evidential large difference. The air sintered Al, Ga co-doped ZnO has higher power factor ($S^2\sigma$) of the order 720.9 μW K^{-2} m^{-1} and lower electrical resistivity (ρ) of 5.803 mΩ cm for the nominal formula $(Zn_{1-x-y}Al_xGa_y)O$, with x = 0.03, y = 0.01 as compared to the power factor 543.6 μW K^{-2} m^{-1} and electrical resistivity of the order 1.550 mΩ cm at 692.2 °C sintered in the argon atmosphere at the same temperature i.e. 1450 °C. The power factor of the air sintered sample with x = 0.03, y = 0.01 is 1.4 times higher than the argon sintered sample with the same composition. The difference in power factors and electrical resistivities are linked to sintering atmospheres. We will investigate the effects of sintering atmospheres of the co-doped ZnO and will study thermoelectric properties, phase, and microstructures of the co-doped ZnO.

1 Introduction

Up to date, ZnO based materials are the best *n*-type thermoelectric materials and are stable at high temperature because of high electrical conductivities and higher Seebeck coefficient. ZnO is among one of the most favorable oxides which have many thermoelectric properties. ZnO has many uses. Its main use in electric power generators [1], sensors and varistors [2, 3]. ZnO is a good thermoelectric material which works in high-temperatures [4, 5]. The forbidden bandgap

of ZnO is 3.5 eV [4]. Boron compounds [5, 6], Si–Ge alloys [7, 8], Selenides and Tellurides [9, 10] have been tested to work at high temperature. For thermoelectric refrigeration superconductor cuprates [11] were also suggested but their performance were affected by their lower carriers mobilities [11, 12]. The only disqualification of ZnO is its high lattice thermal conductivity (κ_l) [4]. ZnO has many uses and applications in chemistry, physics and applied electronics.

So far, different research groups worked on doped ZnO for improving its thermoelectric properties. Teehan et al. in 2011 studied the effect of In doping in ZnO on the electrical resistivity and power factor and succeeded to obtain a power factor of 22.1×10^{-4} WK^{-2} m^{-1} and electrical resistivity of 2.1 mΩ cm [13] In 2010 Berardan et al. studied thermoelectric properties of Al-doped ZnO both in air and N_2 atmosphere and succeeded to achieve a higher power factor 3.9×10^{-4} μW K^{-2} m^{-1} and electrical resistivity 2 mΩ cm under N_2 prepared $(Zn_{1-x}Al_x)$ [14]. Park et al. studied CeO_2 and Dy_2O_3 dual doped ZnO and achieved a power factor 4.46×10^{-4} W K^{-2} m^{-1} at 800 °C [15]. Fan et al. achieved a power factor $(3.11–5.89) \times 10^{-5}$ W K^{-2} m^{-1} for In-doped ZnO [16]. In 2016 Zhang et al. achieved a power factor 6.16×10^{-4} W m^{-1} K^{-2} at 673 K for textured Al/Ni-doped ZnO [17].

✉ Matiullah
  mati.physics1@yahoo.com

✉ C.L. Wang
  wangcl@sdu.edu.cn

[1] School of Physics, Shandong University, Jinan 250100, People's Republic of China

[2] School of Crystal Materials, Shandong University, Jinan 250100, People's Republic of China

[3] Department of Physics, Abdul Wali Khan University, Mardan, K.P.K. 23200, Pakistan

[4] Department of English, Government Degree College Bakshali, Mardan, K.P.K. 23200, Pakistan

In the present work, we have sintered $(Zn_{1-x-y}Al_xGa_y)$ O, in air as well in an argon atmosphere. We have established a relation between thermoelectric properties, phase identification, and microstructure in the air as well in argon atmosphere sintered at 1450 °C for 10 h. We discussed thermoelectric properties in terms of electrical and thermal aspects. We also discussed effects of sintering atmosphere on the c/a lattice ratio.

2 Experimental procedure (Preparation and characterization of samples)

2.1 Samples preparation and characterization

Dual doped (Al, Ga) ZnO powders with ZnO (purity, 99%), Al_2O_3 (purity, 99%) and Ga_2O_3 (purity, 99.99%) were mixed according to the compositions formula $(Zn_{1-x-y}Al_xGa_y)O$, with ($0.02 \leq x \leq 0.04$, $1 \leq y \leq 0.05$). The mixed powders were put in four different container and absolute ethanol was used to prepare slurries of $(Zn_{1-x-y}Al_xGa_y)O$ ceramics, with ($0.02 \leq x \leq 0.04$, $1 \leq y \leq 0.05$). To get homogeneous mixtures the slurries were ball milled via ball milling machine at a milling speed of 205 rpm for 15 h using ethanol as lubricant and zirconia balls as grinders. The slurries of co-doped ZnO were put in a DGX-92438 furnace kept at ~ 105 °C overnight. The slurries were pressed into small pellets of thickness 2 mm with a diameter of 12 mm. The small pellets were pressed via a hand press at 8 MPa. After finishing the pressing of small pellets, all kits were cleaned via absolute ethanol. The small pellets were sintered at 1450 °C for 10 h both in the air as well in the argon atmosphere. The small pellets were cut into column bars 12 mm × 2.0 mm × 2.0 mm for measuring thermoelectric properties. The remaining parts of the small sintered pellets were smashed into small pieces for performing powder for X-ray diffraction and Scanning electron microscopy purposes respectively. The thermoelectric properties like electrical resistivity (ρ), Seebeck coefficient (S) and power factor ($S^2\sigma$) were measured from 100 to 700 °C using LINSEIS Seebeck coefficient and Resistivity unit (LSR-3) machine. The absolute Seebeck coefficient was obtained from relative Seebeck coefficient.

The overall surface structures of all compositions were studied by powder X-ray diffraction (XRD) via a Bruker AXS D8 ADVANCE diffractometer using Cu Kα radiation and scanning (a step width of 0.02°) over the angular range 20°–80°. The XRD and SEM measurements were performed at room temperature. Scanning electron microscope (SEM- Hitachi- S-4800) was used to study surface

topography. The elemental analysis was confirmed via (SEM- Hitachi- S-4800).

2.2 Measurements of thermoelectric properties (S, ρ, power factor)

Thermoelectric properties of all compositions i.e. sintered both in air and argon atmosphere of thickness 2 mm and diameter of 12 mm were cut by the SYJ-160 Low-speed Diamond cutter. To avoid any inconvenience, the air sintered samples were silvered. To measure different thermoelectric properties like electrical resistivity (ρ), Seebeck coefficient (S) and power factor ($S^2\sigma$) were measured by using LINSEIS Seebeck coefficient and resistivity unit LSR-3 (Germany). The Seebeck coefficient obtained from the temperature difference between the upper and lower heaters of the LSR-3 machine. All samples were measured at steady state temperature. The electrical resistivity, Seebeck coefficient and power factor were studied from room temperature to 700 °C. All the data measured via LSR-3 were transferred to a computer system attached to the LSR-3.

3 Results and discussions

For the purpose to know better about the dual doped ZnO structural properties, powder X-rays diffraction of both air and argon sintered atmosphere were performed at 20°–80° using Kuα radiation. Figure 1 shows the observed peaks are corresponding to the host ZnO, hexagonal wurtzite structure and are matching with the PDF # 79-0205, reported data of
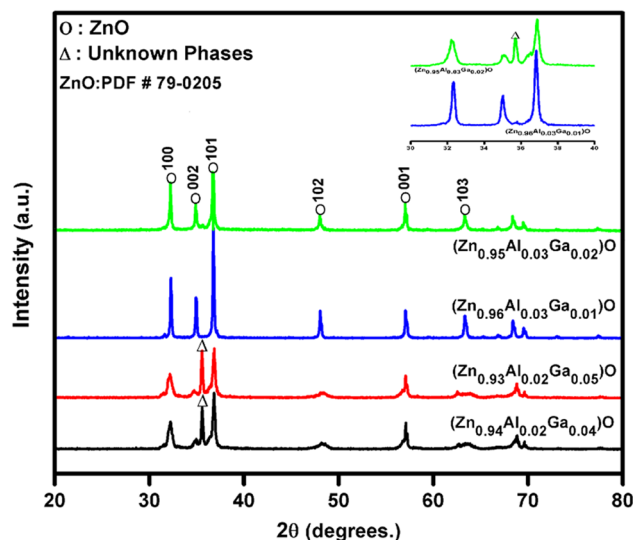

Fig. 1 Powder X-ray diffraction for the nominal formula $(Zn_{1-x-y}Al_xGa_y)$, with x = 0.02, y = 0.04, 0.05 and x = 0.03, y = 0.01, 0.02

the host ZnO. The sharpest peaks are leaning towards the lower values of "d" and show better crystallinity at (101) direction, where (101) are the Miller indices (hkl). Some unknown phases were detected about $2\theta = 35°–37°$. In the inset of Fig. 1, an unknown phase has also been detected for the composition with x = 0.03, y = 0.02, sintered in the air atmosphere. In the argon atmosphere, there are no unknown phases studied for the composition with x = 0.03, y = 0.02.

From XRD results we conclude that host material is strongly affected by Al_2O_3 and Ga_2O_3 concentrations. For 0.01 wt% of Ga, the dopant is critical to possess the high amount of host ZnO. It is clear from Fig. 1 that with the increase of dopant concentrations the (002) magnitude decreases. This means that dopant concentrations are responsible to disturb the crystallinity of the host material [18]. The disturbance of the crystallinity of the host material may be due to the difference of the ionic size between the host and the dopants. The differences between the ionic sizes of the host and dopants create stress and that is the reason that the crystallinity of the host is disturbed. The average particle size can be calculated by Debye Scherer's formula [18] as,

$$D = \frac{0.9\lambda}{\beta\cos\theta} \tag{1}$$

where β is the broadening of the diffraction line, D is the average size of the crystallite size, λ is the wavelength of the X-ray radiation and θ is the Bragg's angle. The undoped ZnO size is 27–36 nm, while the Al_2O_3 doped ZnO average particle size is 10–36 nm [19]. This means that particle size varies with dopants concentrations.

Scanning electron microscope (SEM) images in Fig. 2 shows the surface topography and morphology of different doped ZnO sintered in the air as well in the argon atmosphere. As from XRD results there exist some unknown phases, these unknown phases are becoming lite black due to the excess of Ga concentration. These unknown phases are therefore responsible to increase the electrical resistivities. Figure 2a, b are sintered in air atmosphere. Figure 2a with x = 0.02, y = 0.04 shows that surface is not uniformly distributed and this non-uniform distribution is therefore responsible for high electrical resistivity (ρ). Figure 2b with x = 0.02, y = 0.05 an unknown phase has been observed, indicated by a white arrow. This unknown phase is therefore responsible for high electrical resistivity. Figure 2b is showing porous like structure and this porous structure of the composition with x = 0.02, y = 0.05 is the reason for high electrical resistivity. As Al concentration is same (x = 0.02), while Ga concentration values change from 0.04 to 0.05. The electrical resistivity of both the above-mentioned samples is high which may probably due to excess amount of Ga concentration.

Figure 2c, d are sintered in argon atmosphere where x = 0.03, and y = 0.01, 0.02. The surface of both argon sintered samples are smooth and no unknown or secondary phases were observed. The SEM results of Fig. 2b, c are in good agreement with XRD results. In the XRD there exists no unknown phase as well secondary phase. The absence of secondary and unknown phases, therefore, results in a lower electrical resistivity. The SEM results of Fig. 2b, c are also supported by Fig. 5, i.e. the electrical resistivities

Fig. 2 SEM images for the nominal formula $(Zn_{1-x-y}Al_xGa_y)$, with x = 0.02, y = 0.04, 0.05 and x = 0.03, y = 0.01, 0.02
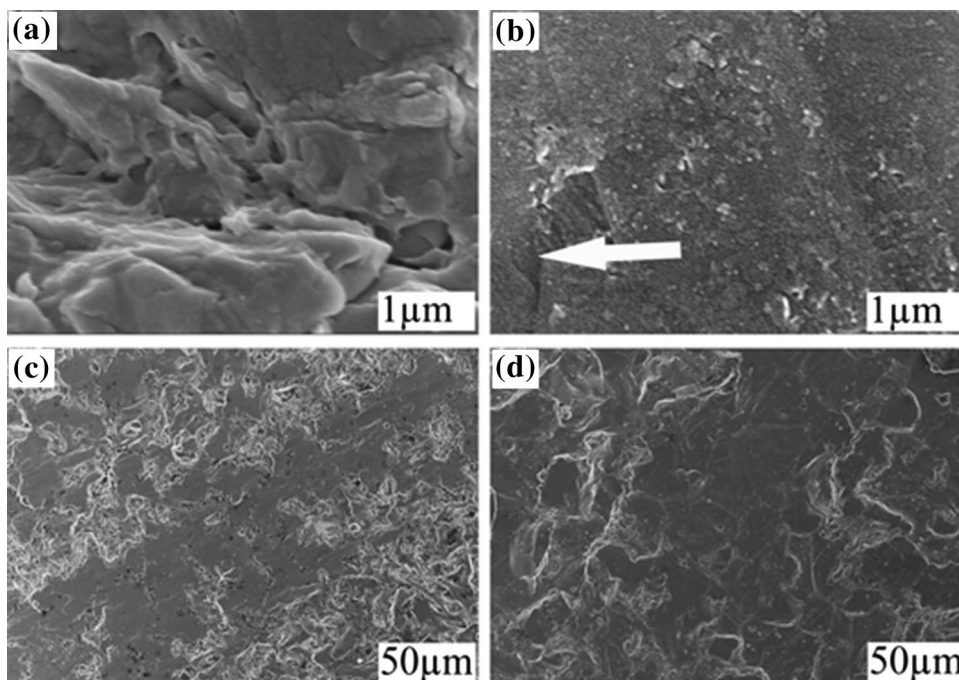
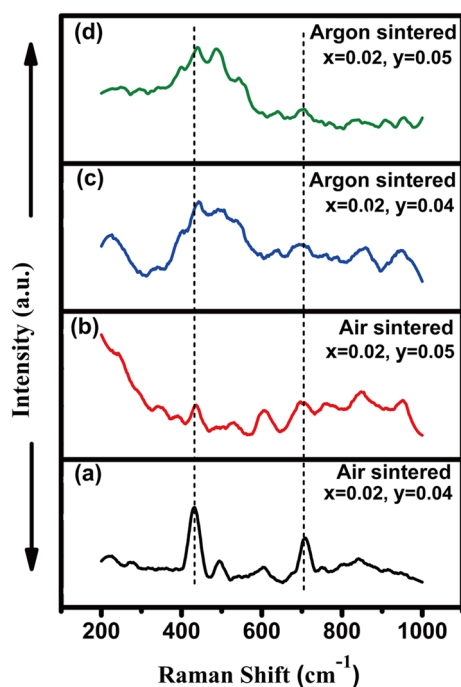**Fig. 3** Raman spectroscopy for the nominal formula $(Zn_{1-x-y}Al_xGa_y)$, with x = 0.02, y = 0.04, 0.05 and x = 0.02, y = 0.04, 0.05 sintered in two different media

of the argon sintered samples are very low compared to air sintered samples.

Figure 3a–d shows room temperature of different doped Raman spectra for $(Zn_{1-x-y}Al_xGa_y)$ ceramics, with x = 0.02, y = 0.04, 0.05 and x = 0.03, y = 0.01, 0.03 in the range 200–1000 cm^{-1}. Figure 3a–d clearly shows the difference between to samples sintered at two different atmospheres (air and argon). These findings are well correlated to our XRD investigations. The peaks are more intense and sharp in air sintered atmosphere compared to the peaks (c, d) and spectra sintered at argon atmosphere, resulted in a lower value of Seebeck coefficient and electrical resistivities. The highest and sharpest peak occurs at 430 cm^{-1}. Small shifting of peaks along with the decrease of intensities at higher concentration indicates the incorporation of Al and Ga.

Figure 4 confirms the the presence of compositions used for preparing samples (elemental analysis). The figure confirms the compositions existence, which was obtained via (SEM- Hitachi- S-4800) are pure. The elemental analysis mapping also provides the % weight of oxygen, Zinc, Al, and Ga. All values obtained from the elemental mapping are shown in the Table 1.

Figure 5 shows resistivity of the nominal formula $(Zn_{1-x-y}Al_xGa_y)O$, with $(0.02 \leq x \leq 0.04, 1 \leq y \leq 0.05)$ as a function of temperature. Undoped ZnO is a semiconductor with a large band gap and has poor electrical conductivity [14]. The addition of Al and Ga is to enhance the electrical

conductivity of undoped ZnO [4]. Electrical resistivity is a function of temperature and changes occur clearly in resistivity with increasing temperature. The temperature increases linearly with increases in temperature from 100 to 700 °C. As clear from the Fig. 4 the electrical resistivity of the argon atmosphere is rather very low as compared to the air sintered samples and the maximum value of argon sintered atmosphere increases from 0.611 to 0.973 mΩ cm at 104.6 to 693.1 °C. The electrical resistiviries of air sintered samples are clearly high and even the lowest resistivity of the air sintered samples increases from 5.067 mΩ cm at 123.1 °C to 5.803 mΩ cm at 702.5 °C, which is significantly high for the same composition (x = 0.02, y = 0.01) sintered in the argon atmosphere. As observed from Fig. 5 the air sintered samples electrical resistivities are significantly high than the samples sintered in the argon atmosphere. For argon sintered samples the electrical resistivities are low due to the higher number of charge carriers. With the increasing number of charge carrier concentration, the absolute value of Seebeck coefficient will be decreased. From the Fig. 5, it is evident that electrical resistivities of the air sintered samples decreases with increasing temperature, showing semiconductor behavior. Such situation in which electrical resistivity of a semiconductor decreases with increasing temperature is known as negative coefficient of temperature (NTC) [20]. This increase in electrical resistivities with increase in temperature shows metallic behavior. The sample shows semiconductor to metallic transition (SMT) [21, 22]. Looking at Fig. 5 the electrical resistivity of argon sintered atmosphere there occur an increase in electrical resistivities, showing metallic behavior of the samples.

It has been studied that electrical resistivities of argon sintered samples are increasing with the increase of temperature (Fig. 5), positive coefficient of temperature (PTC) [22]. The number of carriers is low because the Fermi level carriers cannot jump to the conduction band may cause the possibility of decrease in electrical resistivities.

Figure 6 shows Seebeck coefficient depends on temperature very clearly. The Seebeck effect occurs whenever there is a temperature difference between two ends of a semiconductor. The Seebeck coefficient values of all the compositions are negative over the whole temperature, indication *n*-type conduction [23].The negative values of Seebeck coefficient are in good agreement; that conduction is dominated by electron carriers [24]. The absolute value of Seebeck coefficient has lower values for x = 0.03, y = 0.01, 0.02. The lower values of Seebeck coefficient for the two mentioned samples is due to the higher concentration and incomplete densification of the particles inside the sample [25]. It should be noted that the composition y = 0.02, on the left side of Fig. 2a has a heterogeneous texture and possesses the highest Seebeck coefficient value − 225.18 µV K^{-1} at 702.2 °C. With the increase of Ga concentration, the number of carriers concentration increased
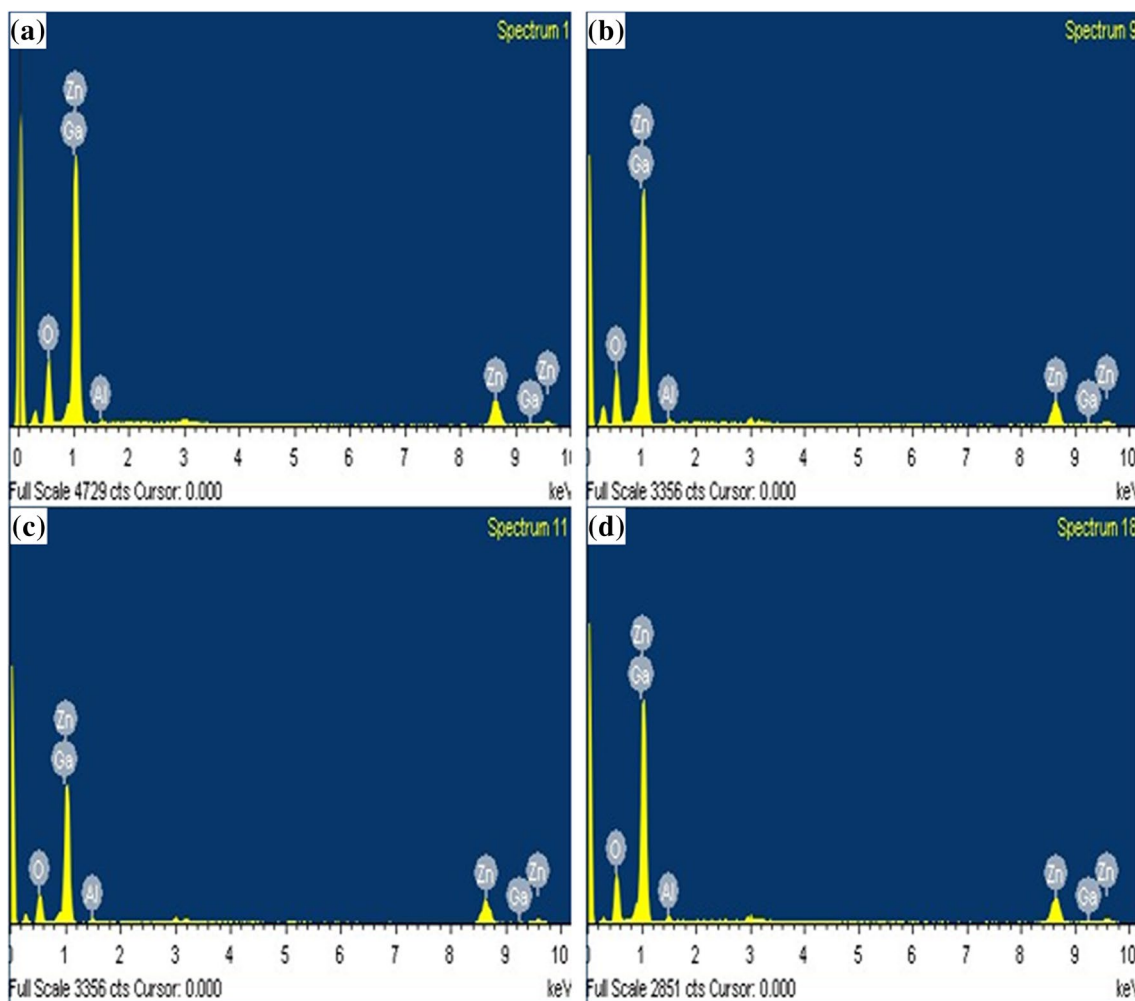
Fig. 4 Elemental analysis for the nominal formula $(Zn_{1-x-y}Al_xGa_y)$, with $x = 0.02$, $y = 0.04$, 0.05 and $x = 0.03$, $y = 0.01$, 0.02

Table 1 Weight % of Al, Ga, Zn and oxygen

Compositions	Zinc wt%	Al wt%	Ga wt%	Oxygen wt%	Total
$x = 0.03$, $y = 0.01$	50.97	2.29	1.59	45.15	100
$x = 0.03$, $y = 0.02$	43.80	2.36	1.95	51.89	100
$x = 0.02$, $y = 0.04$	42.66	1.15	3.59	52.60	100
$x = 0.02$, $y = 0.05$	42.37	1.42	4.28	51.93	100

and hence Seebeck coefficient decreased. The maximum value of Seebeck coefficient has been studied for the samples with $x = 0.03$, $y = 0.02$ of the order -225.18 µV K^{-1} at 702.2 °C. The Seebeck coefficient can be expressed by Jokers relation [26] as,
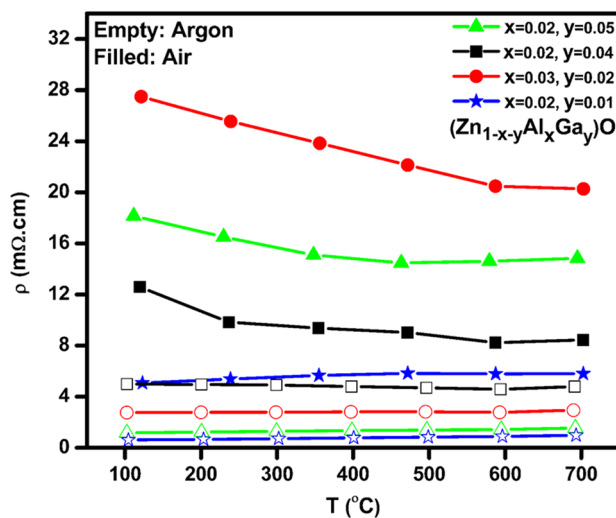
$$S = ATm^* \left(\frac{\pi}{3n} \right)^{\frac{2}{3}}$$
(2)

Fig. 5 Electrical resistivity of the nominal formula $(Zn_{1-x-y}Al_xGa_y)$, with $x = 0.02$, $y = 0.04$, 0.05 and $x = 0.03$, $y = 0.01$, 0.02
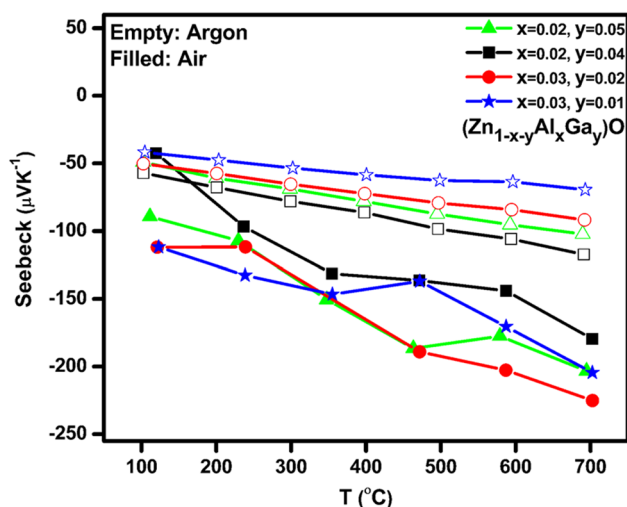
Fig. 6 Seebeck coefficient of the nominal formula $(Zn_{1-x-y}Al_xGa_y)$, with $x = 0.02$, $y = 0.04$, 0.05 and $x = 0.03$, $y = 0.01$, 0.02

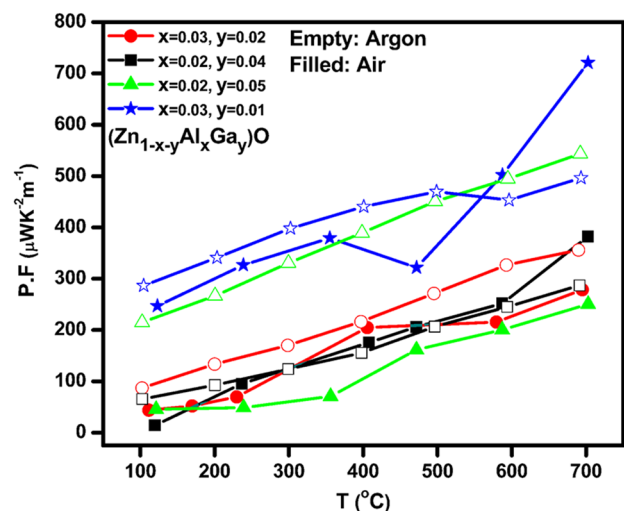**Table 2** The lattice parameters for $(Zn_{1-x}Al_xGa_Y)O$, with $x = 0.03$, 0.02, $y = 0.1$, 0.02, 0.05 and 0.05 sintered in air

Compositions	a (Å)	c (Å)	c/a
x = 0.03, y = 0.01	3.21594	5.21210	1.6191
x = 0.03, y = 0.02	3.23108	5.16732	1.5992
x = 0.02, y = 0.04	3.23826	5.18418	1.6009
x = 0.02, y = 0.05	3.23098	5.10961	1.5814

Table 3 The lattice parameters for $(Zn_{1-x}Al_xGa_Y)O$, with $x = 0.03$, 0.02, $y = 0.4$, 0.05, 0.01 and 0.02 sintered in argon

Compositions	a (Å)	c (Å)	c/a
x = 0.03, y = 0.01	3.23842	5.18785	1.6019
x = 0.03, y = 0.02	3.23033	5.17300	1.6013
x = 0.02, y = 0.04	3.22902	5.12595	1.5874
x = 0.02, y = 0.05	3.22590	5.13812	1.5927

Fig. 7 Power factor of the nominal formula $(Zn_{1-x-y}Al_xGa_y)$, with $x = 0.02$, $y = 0.04$, 0.05 and $x = 0.03$, $y = 0.01$, 0.02

where n is the charge carrier concentration, A is constant, T is absolute temperature and $m*$ is mass of the carriers at Fermi level. For argon sintered the Seebeck coefficient is very low compared to air sintered samples. The reason for the lower value of Seebeck coefficient for argon sintered samples is due to the higher number of charge carriers. The higher the Seebeck coefficient and lower electrical resistivity will yield a higher power factor. From SEM images (Fig. 2a, b) the samples with $x = 0.02$, $y = 0.4$, 0.05 there exists porous like structure and for such structures, there will occur a strong decadence in the electrical conductivity (σ) and hence the power factor will result in lower values shown in Fig. 7.

From Fig. 2a, b the SEM images for $x = 0.02$, $y = 0.04$, 0.05, the electrical resistivity of the air sintered samples is very high (Table 2). Figure 7a, b establishes a relation between electrical resistivities and Seebeck coefficients for both air as well argon sintered samples. For composition with $x = 0.03$, $y = 0.01$, 0.02 (argon sintered), there exists no unknown as well secondary phases (Fig. 2). The general trend of lower Seebeck coefficient is the higher number of charge carriers. As in argon sintered atmosphere, the Seebeck coefficient of the measured samples is low, which is attributed to the higher number of carrier's concentration. The relation between Seebeck coefficient and electrical resistivity has shown in Fig. 8a, b. Tables 1 and 2 are the lattice parameters a and c of $(Zn_{1-x-y}Al_xGa_y)O$ ceramics, with $x = 0.02$, 0.03 and $y = 0.01$, 0.02, 0.04, 0.05 sintered in argon (Table 2) and air atmosphere (Table 3). From Tables 2 and 3 it is evident that lattice parameters c/a ration also affected by different sintering media. As electrical resistivity, Seebeck coefficient and power factor all are temperature as well sintering media dependent, similarly lattice constants are also function of temperature. From Tables 2 and 3 it is evident that lattice constants are sintering media dependents.

Figure 7 shows a relationship between power factor and temperature. Power factor increases with increase in temperature. Power factor, $S^2\sigma$, shows the overall electrical contribution of the material. As we have observed in the SEM images that the Ga concentration with 0.04, 0.05 the excess amount of Ga is responsible for the unknown phases, the structure also looking very similar to a porous structure and for a porous like structure, the electrical conductivity will be low. The lower value of electrical conductivity is therefore attributed to a lower power factor, $S^2\sigma$, where S is the Seebeck coefficient and σ is the electrical conductivity,
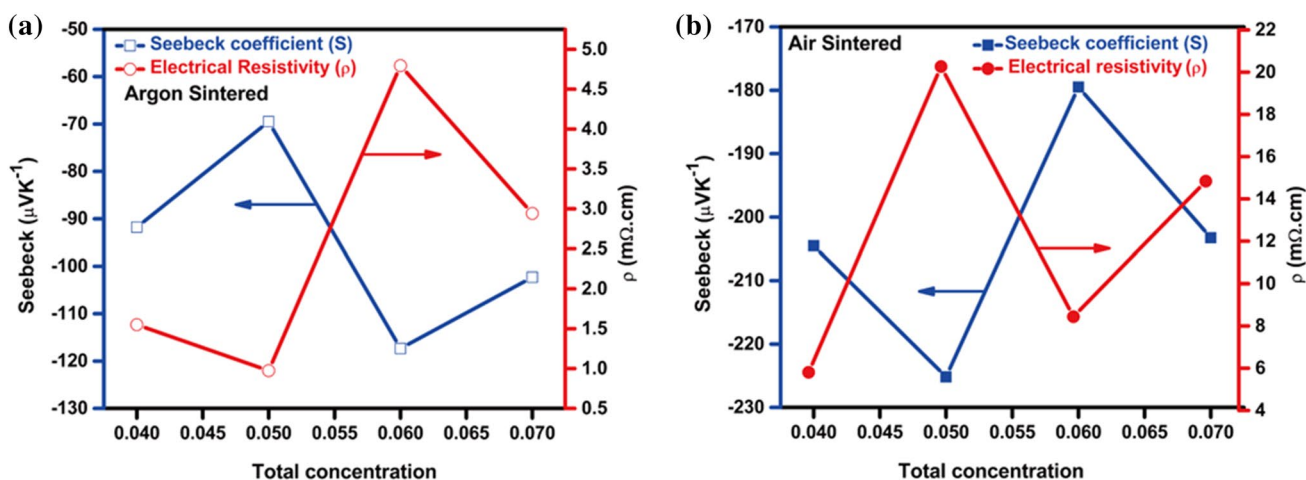
Fig. 8 **a, b** Relation between Seebeck coefficient and electrical resistivity of the nominal formula $(Zn_{1-x-y}Al_xGa_y)$, with x = 0.02, y = 0.04, 0.05 and x = 0.03, y = 0.01, 0.02

reciprocal of electrical resistivity (ρ). The power factor depends more on Seebeck coefficient as compared to electrical resistivity [27]. The higher the Seebeck coefficient value and lower electrical resistivity, the higher will be the resultant power factor. Power factor can be expressed [28] as,

$$P.F = S^2\sigma \tag{3}$$

where P.F stands for power factor, S is the absolute Seebeck coefficient and σ is the electrical conductivity. The sample for which x = 0.03, y = 0.01 shows the highest value of power factor, its value increases from 246.9 µW K^{-2} m^{-1} at 123.1 °C to 720.9 µW K^{-2} m^{-1} at 702.5 °C. The same composition sintered in argon atmosphere resulting in a power factor of the order 543.6 µW K^{-2} m^{-1}. There is a clear difference between power factor obtained in air and in argon. The reason for the lower value of power factor is due to

the lower value of Seebeck coefficient studied in the argon atmosphere. As the Seebeck coefficient observed in argon atmosphere has lower value but its electrical resistivity is very low as compared to those samples sintered in the argon atmosphere.

The power factor of argon sintered samples is ~ 1.4 times smaller than those of air sintered samples. The reason for the lower power factor of argon sintered samples is the higher number of charge carriers (n), the higher number of (n) will restrict the Seebeck value (Eq. 2) as a result, the power factor results in lower values.

Figure 9a, b shows that power factor (S^{2}σ), is a function of c/a lattice ratio. The higher the c/a lattice ratio, the higher will be the power factor [29]. Figure 9a establishes a relation between c/a lattice ratio and power factor sintered in air atmosphere, while Fig. 9b shows a relation between c/a
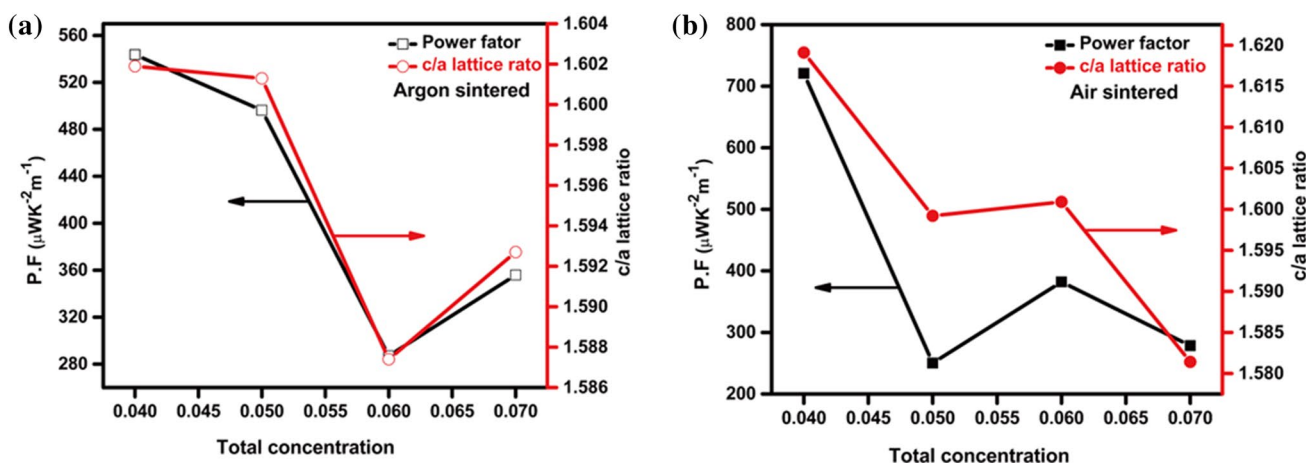

Fig. 9 **a, b** Relation between power factor and c/a lattice ratio of the nominal formula $(Zn_{1-x-y}Al_xGa_y)$, with x = 0.02, y = 0.04, 0.05 and x = 0.03, y = 0.01, 0.02
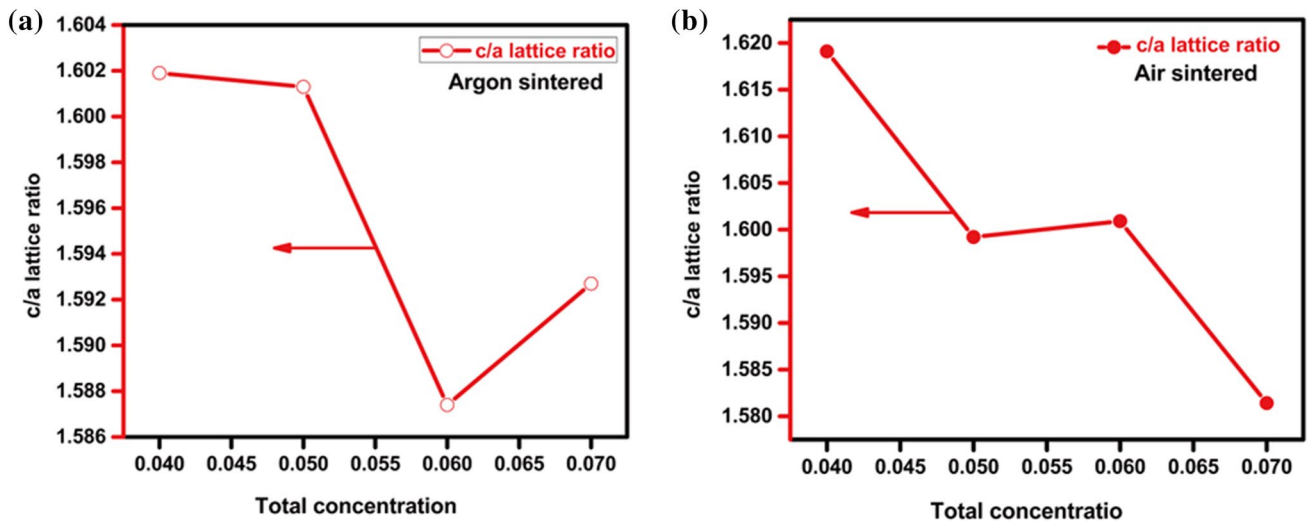
Fig. 10 Variation of c/a lattice ratio with Al, Ga values for the nominal formula $(Zn_{1-x-y}Al_xGa_y)$, with x = 0.02, y = 0.04, 0.05 and x = 0.03, y = 0.01, 0.02

lattice ratio and power factor for those samples sintered in the argon atmosphere. We observed that for both sintering atmospheres the power factor changes with change in c/a lattice ratio.

Figure 10 reveals that c/a lattice ration for the samples with x = 0.03, y = 0.01 has good values for both sintering media (air and argon). Though the c/a lattice ratio for the sample with x = 0.03, y = 0.02 is high than the sample with x = 0.03, y = 0.01 but due to high electrical resistivity (ρ), of the sample (x = 0.03, 0.02), will result in a lower power factor.

4 Conclusions

Al, Ga co-doped ZnO were mixed according to nominal formula $(Zn_{1-x-y}Al_xGa_y)O$. All samples were sintered in the air as well in the argon atmosphere. It has been proved that power factor of air sintered compositions is higher than those of argon sintered samples. The electrical resistivities of argon sintered samples studied were found to be very low than air sintered samples. The Seebeck coefficient and power factor of air sintered studied have higher values compared to argon sintered samples. The powder X-ray diffraction (XRD) of both air sintered and argon sintered atmosphere are different. In air sintered atmosphere the number of unknown phases are greater in number than those of argon sintered samples. The electrical resistivities of argon sintered atmosphere samples are very low than those of air sintered atmosphere. It has been observed that Seebeck coefficient and electrical resistivity of argon sintered samples have lower values than those of air sintered samples. The power factors obtained for air sintered samples have higher

values than those samples sintered in the argon atmosphere. We conclude that phase, microstructure and thermoelectric properties of the co-doped ZnO both sintered in air and argon atmosphere at 1450 °C, are different. It has been studied that lattice parameters c/a ratios were affected by different sintering atmospheres. Finally, for air sintered samples 1.4 times higher power factor (than argon sintered samples) 720.9 $\mu W\ K^{-2}\ m^{-1}$ at 702.5 °C is obtained for $(Zn_{1-x-y}Al_xGa_y)O$ ceramics, with x = 0.03, y = 0.01.

References

1. Z.L. Wang, J. Song, Science **312**, 242 (2006)
2. J. Xu, J. Han, Y. Zhang, Y. Sun, B. Xie, Sens. Actuators B **132**, 334 (2008)
3. F. Jiang, Z. Peng, Y. Zhang, X. Fu, J. Adv. Ceram. **2**, 201 (2013)
4. T. Tsubota, M. Ohtaki, K. Eguchi, H. Arai, J. Mater. Chem. **7**, 85 (1997)
5. C. Wood, D. Emin, Phys. Rev. B **29**, 4582 (1984)
6. S. Yugo, T. Sato, T. Kimura, Appl. Phys. Lett. **46**, 842 (1985)
7. G. Joshi, H. Lee, Y. Lan, X. Wang, G. Zhu, D. Wang, R.W. Gold, D.C. Cuff, M.Y. Tang, M.S. Dresselhaus, G. Chen, Z. Ren, Nano Lett. **8**, 4670 (2008)
8. X.W. Wang, H. Lee, Y.C. Lan, G.H. Zhu, G. Joshi, D.Z. Wang, J. Yang, A.J. Muto, M.Y. Tang, J. Klatsky, S. Song, M.S. Dresselhaus, G. Chen, Z.F. Ren, Appl. Phys. Lett. **93**, 193121 (2008)
9. V.F. Litvinenko, A.R. Kopan, Powder Metall. Met. Ceram. **48**, 77 (2009)

10. J.F. Nakahara, T. Takeshita, M.J. Tschetter, B.J. Beaudry, K.A. Gschneidner Jr., J. Appl. Phys. **63**, 2331 (1988)
11. W. Macklin, P. Moseley, Mater. Sci. Eng. B **7**, 111 (1990)
12. T.O. Mason, Mater. Sci. Eng. B **10**, 257 (1991)
13. S. Teehan, H. Efstathiadis, P. Haldar, J. Alloys Compd. **509**, 1094 (2011)
14. D. Bérardan, C. Byl, N. Dragoe., J. Am. Ceram. Soc. **93**, 2352 (2010)
15. K. Park, H.K. Hwang, J.W. Seo, W.S. Seo, Energy **54**, 139 (2013)
16. L. Fang, X.F. Yang, L.P. Peng, K. Zhou, F. Wu, Q.L. Huang, C.Y. Kong, J. Supercond. Nov. Magn. **23**, 889 (2010)
17. D.B. Zhang, B.P. Zhang, D.S. Ye, Y.C. Liu, S. Li, J. Alloys Compd. **656**, 784 (2016)
18. U. Holzwarth, N. Gibson, Nat. Nanotechnol. **6**, 534 (2011)
19. M. Deore, G. Jain, Int. J. Nanopart. **7**, 57 (2014)
20. M.A.L. Nobre, S. Lanfredi, Appl. Phys. Lett. **82**, 2284 (2003)
21. O. Bamiduro, H. Mustafa, R. Mundle, R.B. Konda, A.K. Pradhan, Appl. Phys. Lett. **90**, 252108 (2007)
22. L. Hui, Q. Hong, Y. Mingpeng, C. Xiaobai, Mater. Chem. Phys. **126**, 866 (2011)
23. S.B. Zhang, S.H. Wei, A. Zunger, Phys. Rev. B **63**, 075205 (2001)
24. H. Colder, E. Guilmeau, C. Harnois, S. Marinel, R. Retoux, E. Savary, J. Eur. Ceram. Soc. **31**, 2957 (2011)
25. L. Han, L.T. Hung, N.V. Nong, N. Pryds, S. Linderoth, J. Electron. Mater. **42**, 1573 (2013)
26. Y. Kinemuchi, C. Ito, H. Kaga, T. Aoki., J. Mater. Res. **22**, 1942 (2007)
27. S. Katsuyama, Y. Takagi, M. Ito, K. Majima, H. Nagai, J. Appl. Phys. **92**, 1391 (2002)
28. K.H. Jung, K.H. Li, W.S. Seo, S.M. Choi, Appl. Phys. Lett. **100**, 253902 (2012)
29. J.P. Wiff, Y. Kinemuchi, H. Kaga, C. Ito, K. Watari, J. Eur. Ceram. Soc. **29**, 1413 (2009)